Physical and Optical Properties of Al /Yb-dually incorporated CuS Particles Prepared by Facile Co-precipitation Process

Pakkawat Nimitnopphasit[1], Junkrajang Wattana[1], Thanaphon Kansaard[1], Wanichaya Mekprasart[1], Kanokthip Boonyarattanakalin[1], C.K. Jayasankar[2], and Weerachon Phoohinkong[3,*]

[1]*College of Materials Innovation and Technology, King Mongkut's Institute of Technology Ladkrabang, Bangkok, 10520, Thailand*
[2]*Department of Physics, Sri Venkateswara University, Tirupati - 517 502, India*
[3]*Faculty of Science and Technology, Suan Dusit University, Bangkok, 10300 Thailand*

Received: 9 October 2024, Revised: 22 December 2024, Accepted: 24 December 2024

Abstract

Energy conservation and management are critical areas of research, particularly in the development of materials for near-infrared (NIR) shielding to reduce energy consumption in buildings. Copper (II) sulfide (CuS), a p-type semiconductor with promising NIR shielding properties, can be further enhanced through appropriate elemental doping. This study reports the synthesis of Al and Yb dual-doped CuS particles using a simple co-precipitation method. The effects of Al and Yb doping on the structural and optical properties of CuS were investigated using X-ray diffraction (XRD), field-emission scanning electron microscopy (FE-SEM), energy-dispersive X-ray spectroscopy (EDX), and UV–Vis–NIR spectroscopy. The results reveal that Al and Yb dopants significantly enhance the material's physical and optical properties, particularly in the NIR spectral region. The optimized doping composition achieved superior NIR shielding performance, making these materials highly suitable for energy-saving applications.

Keywords: CuS, Al and Yb doping, co-precipitation method, NIR shielding, Energy efficiency

1. Introduction

The efficient management of energy resources is a pressing challenge in contemporary society. One strategy to mitigate energy consumption in buildings is the incorporation of materials with near-infrared (NIR) shielding properties into windows and coatings [1]-[4]. Copper (II) sulfide (CuS) is a p-type semiconductor with a narrow bandgap (approximately 2.0 eV) that exhibits excellent optical absorption in the NIR range. The relevant optical properties of copper sulfide-based material strongly depend on the stoichiometry of different copper sulfide phases (e.g. Chalcocite (Cu_2S), djurleite ($Cu_{1.9}S$), digenite ($Cu_{1.8}S$), aniline ($Cu_{1.75}S$) and covellite (CuS) [5]. It is widely used as a photocatalyst, cathode material, and thermal insulation material that can be proposed for optical filter for energy-saving [6]-[7]. However, the optical performance and physical properties of CuS can be significantly improved through elemental doping.

Aluminum (Al) and ytterbium (Yb) have been identified as effective dopants for CuS due to their ability to alter the electronic structure and enhance NIR absorption. Al is a trivalent metal ion capable of substituting Cu^{2+} ions in the lattice, introducing charge carriers and modulating the band structure. Al leading to increasing p-type characteristics and further induced strong infrared absorptivity. Yb, a rare earth element, contributes through its unique electronic configuration with strong absorption at 980 nm due to the transition between $^2F_{7/2}$ and $^2F_{5/2}$, energy, which may enhance the optical activity of the host material. The dual-doping approach aims to synergistically improve the NIR shielding performance of CuS particles while maintaining structural stability.

This study focuses on the synthesis of Al/Yb dual-doped CuS particles via a facile co-precipitation method. The structural, morphological, and optical properties of the synthesized materials were characterized to evaluate their potential for energy-efficient applications.

Corresponding Author: weerachon_pho@dusit.ac.th

2. Experimental Methods

2.1 Materials and synthesis of Al/Yb Dual-Doped CuS

Thiourea (CH_4N_2S), triethanolamine (TEA), Copper (II) nitrate trihydrate ($Cu(NO_3)_2$), Ytterbium(lll) Nitrate pentahydrate ($Yb(NO_3)_3)\cdot5H_2O$) and Aluminium (III) nitrate nonahydrate ($Al(NO_3)_3\cdot9H_2O$) were utilized for the development of the Al: Yb: CuS samples. In a typical co-precipitation synthesis, 0.1 mol of $Cu(NO_3)_2$, 0.02 mol ($Yb(NO_3)_3)\cdot5H_2O$) and designated amounts of ($Al(NO_3)_3\cdot9H_2O$) was added into 50 ml of deionized water then 4 ml of TEA and 8 ml of isopropyl alcohol were added and stirred vigorously for 30 min at 70 °C (pH = 8). The Yb content in the precursor was fixed at 2 mol% and Al composition was varied for 2 mol%, 4 mol%, 6 mol% and 8 mol%. This mixture was labelled as Yb/Al/Cu -precursor solution. Next, 0.1 mol of CH_4N_2S was added directly into the Yb/Al/Cu -precursor solution. Then, the total volume of this solution was made up to 200 ml by adding deionized water and the pH of the solution was maintained at ~10 by adding NH_3 solution. The mixture was allowed to react for 2 h at a constant temperature of 70 °C. After the reaction, the solution was cooled naturally to room temperature. A greenish-black precipitate was obtained, which was collected and washed successively with distilled water three times to remove the by-products and impurities. Finally, the obtained product was dried overnight in an oven at 100 °C.

2.2 Characterization Techniques

X-ray diffraction (XRD, Rigaku Smartlab X-ray diffractometer) was utilized to determine the crystalline structure of the samples. Field-emission scanning electron microscopy (FE-SEM, JEOL JSM-7610F) coupled with energy-dispersive X-ray spectroscopy (EDX) was employed to analyze the morphology and elemental composition. UV–Vis–NIR spectroscopy was used to measure the optical properties, including the NIR shielding performance. The energy-saving efficiency of Al/Yb co-doped CuS was evaluated by a home-made device. A simulated house with top opening was built (Fig. 1). The coated glasses with as-prepared samples were placed on the top of the box, which was irradiated by a 100 W infrared lamp. The indoor temperature of the heat box was recorded by an electronic thermometer.

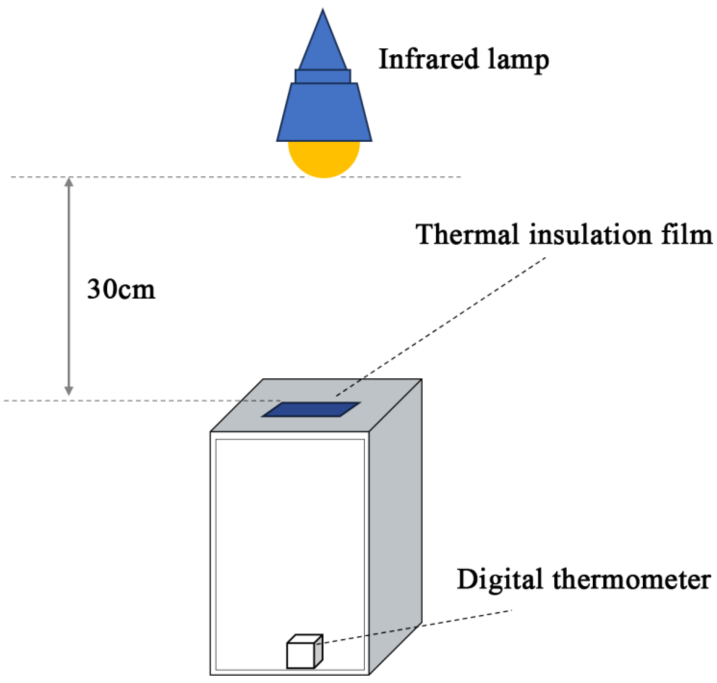

Fig. 1. Schematic diagram of the device used for the thermal insulation test.

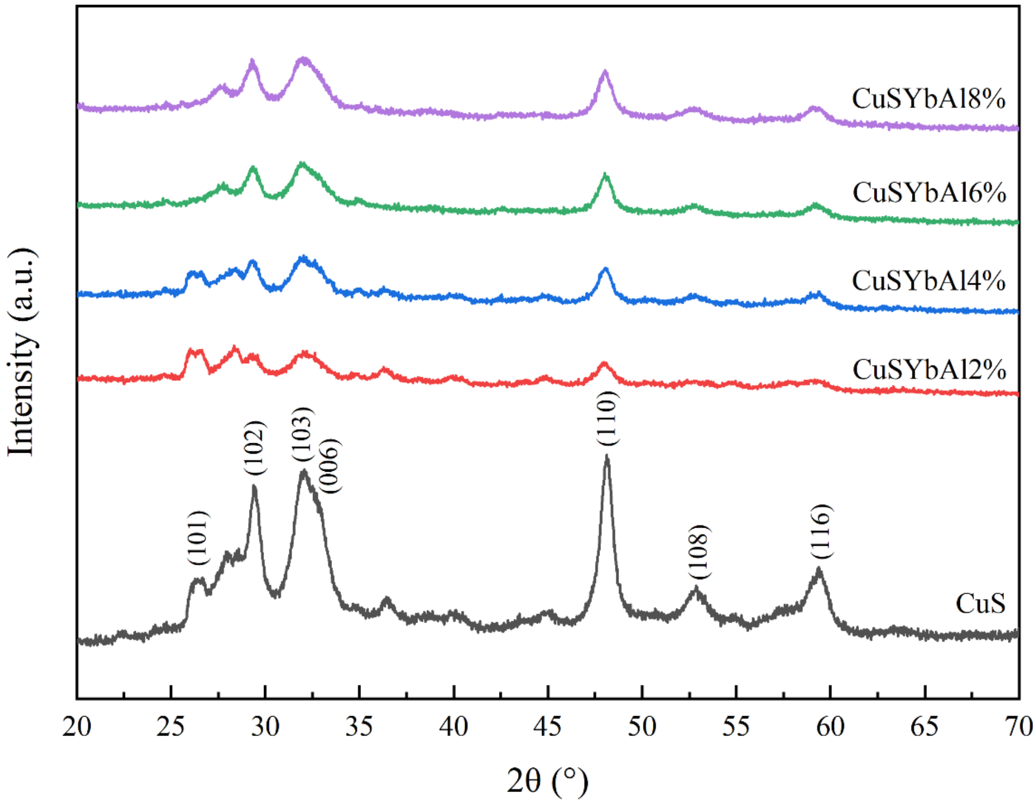

Fig. 2. XRD patterns of Al/Yb co-doped CuS with different Al doping contents.

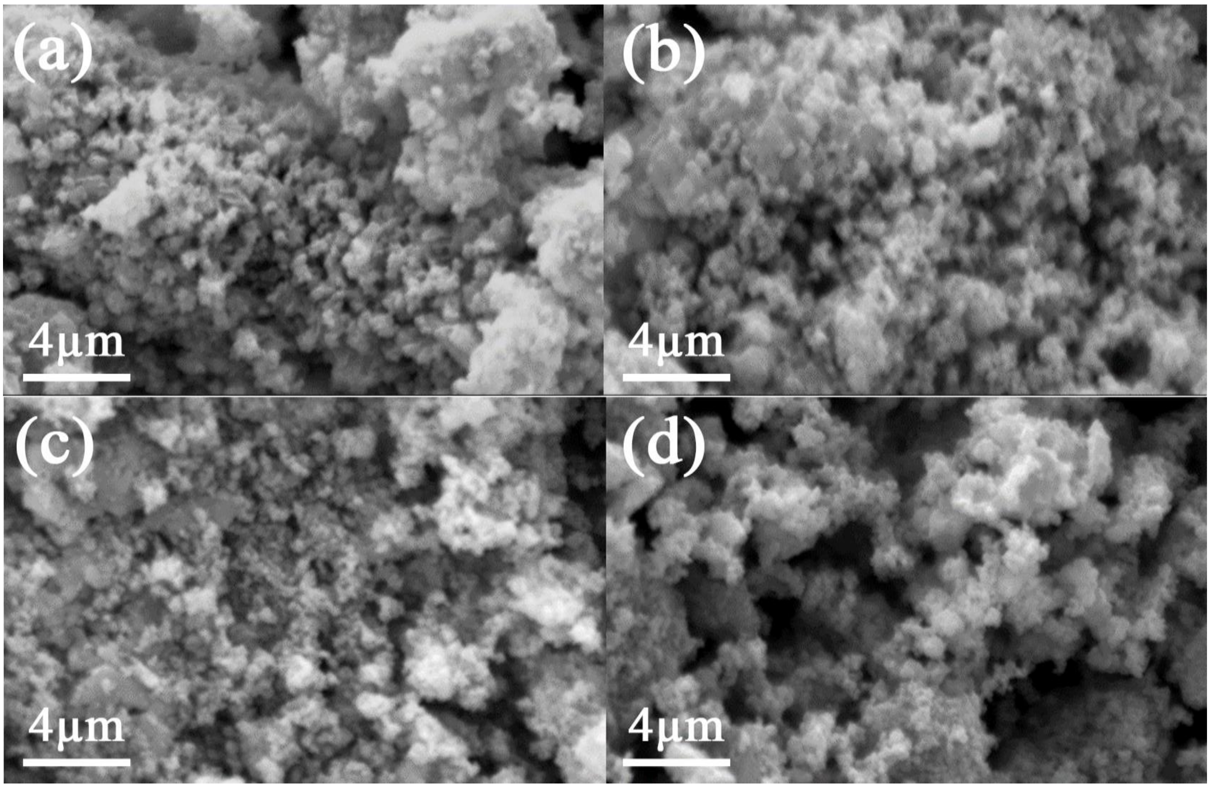

Fig. 3. (a) SEM image of 2mol% Al/Yb co-doped CuS, (B) 4 mol% Al/Yb: CuS, (c) 6 mol% Al/Yb: CuS, and (d) 8mol% Al/Yb: CuS powder.

3. Result and discussion

3.1 Structural analysis

The XRD patterns of the synthesized Al/Yb co-doped CuS with different doping amounts are shown in Fig. 2. The locations of the diffraction peaks corresponded to those of the hexagonal covellite crystalline CuS structure and are matched with standardized JCPDS No. 06-0464 [8]. On the basis of 2θ, the diffraction peaks associated with the (101), (102), (103), (006), (110), (108) and (116) miller planes were found to be at 27.68º, 29.25º, 32.82º, 49.94º, 52.67º and 59.27º, respectively. Furthermore, the incorporation of Al and Yb dopants resulted in slight shifts in peak positions towards a lower angle, indicating lattice distortion due to the substitution of larger ionic radii Al^{3+} and Yb^{3+} ions for Cu^{2+} ions in the octahedral coordination. This substitution increases the average interplanar spacing [9]-[10], confirming the successful incorporation of Al/Yb ions into the hexagonal CuS lattice [11]. No secondary phases corresponding to Al or Yb oxides were detected, confirming successful incorporation of dopants into the CuS lattice. The introduction of these dopants with charge imbalance may also induce lattice defects, contributing to the observed peak shift.

3.2 Morphological and Compositional Analysis

Scanning electron microscope (SEM) photographs of the synthesized CuS and Al/Yb-doped CuS samples were collected to analyze the surface characteristics as displayed in Fig. 3. It is observed that all the samples are generally composed of primary nanoparticles that are aggregated to form larger structures. As Observed in Fig. 4, EDX analysis confirmed the presence of Cu, S, Al, and Yb in the samples, with elemental distributions consistent with the intended doping concentrations. The uniform distribution of dopants was evident from the elemental mapping.

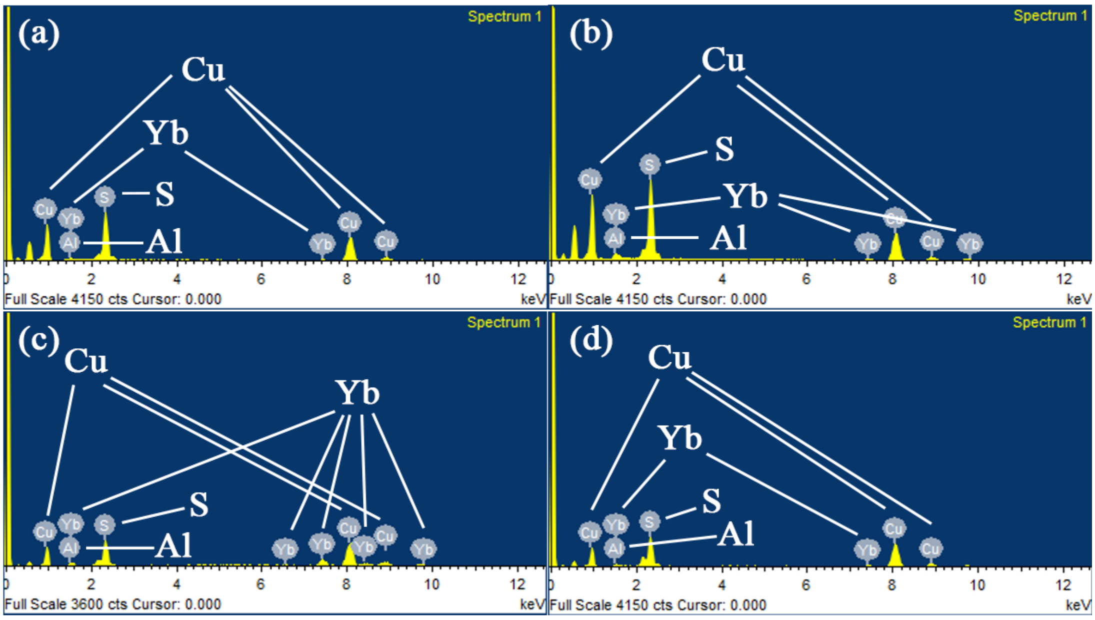

Fig. 4. (a) EDX spectrum of 2 mol% Al/Yb co-doped CuS, (b) 4 mol% Al/Yb: CuS, (c) 6 mol% Al/Yb: CuS, and (d) 8 mol% Al/Yb: CuS.

Table 1. Comparison of Cu^{+}/Cu^{2+} ratios and optical band gap between CuS and Yb-Al co-doped CuS particles.

Sample	CuS	CuSYb2%	CuSYbAl2%	CuSYbAl8%
Cu^{+}/Cu^{2+}	2.66	1.68	3.12	0.83
Band gap (eV)	2.30	2.28	2.27	2.29

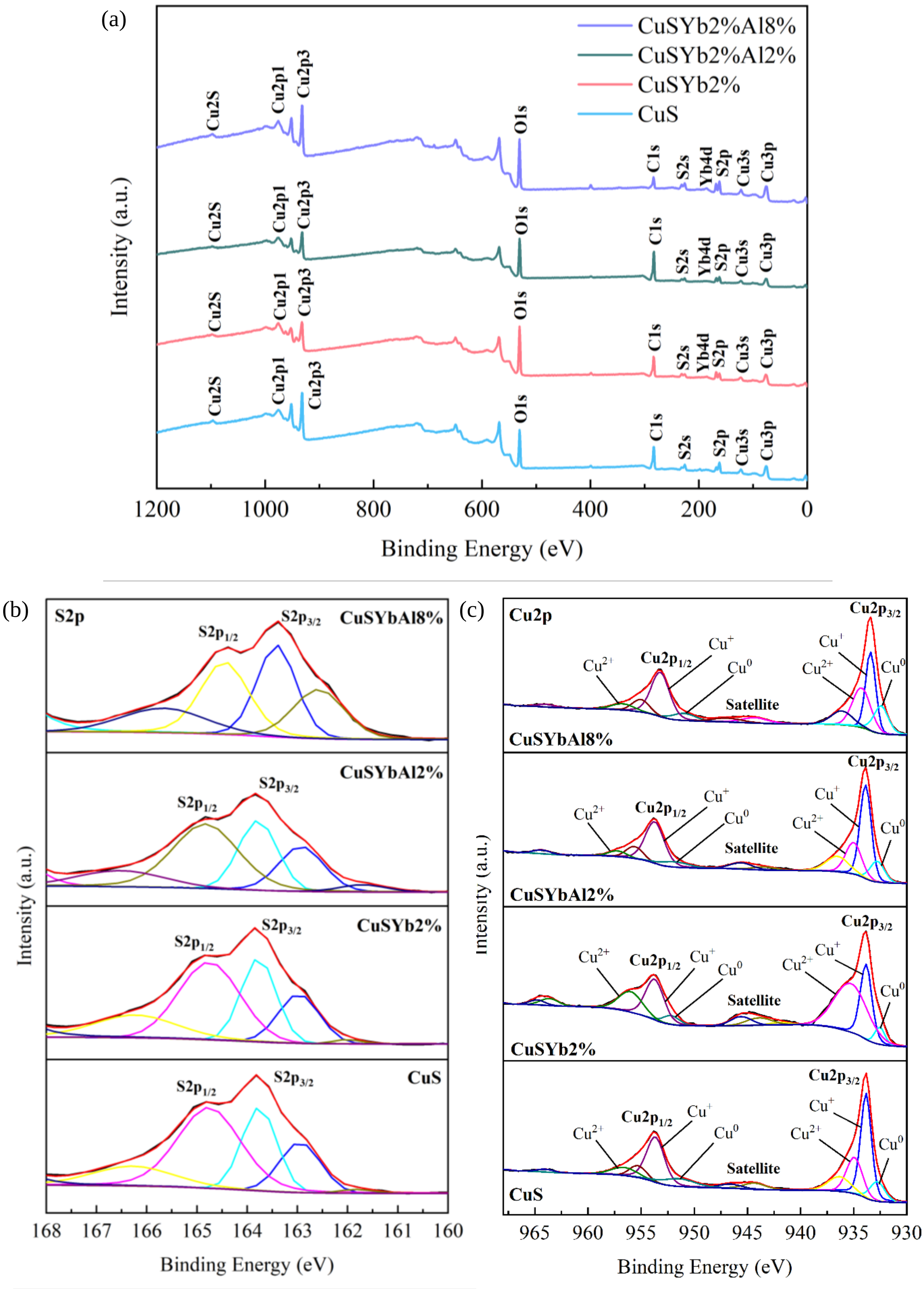

Fig. 5. Survey scan and high-resolution spectra for S 2p and Cu 2p oxidation states of as-prepared CuS and Yb/Al co-doped CuS nanoparticles

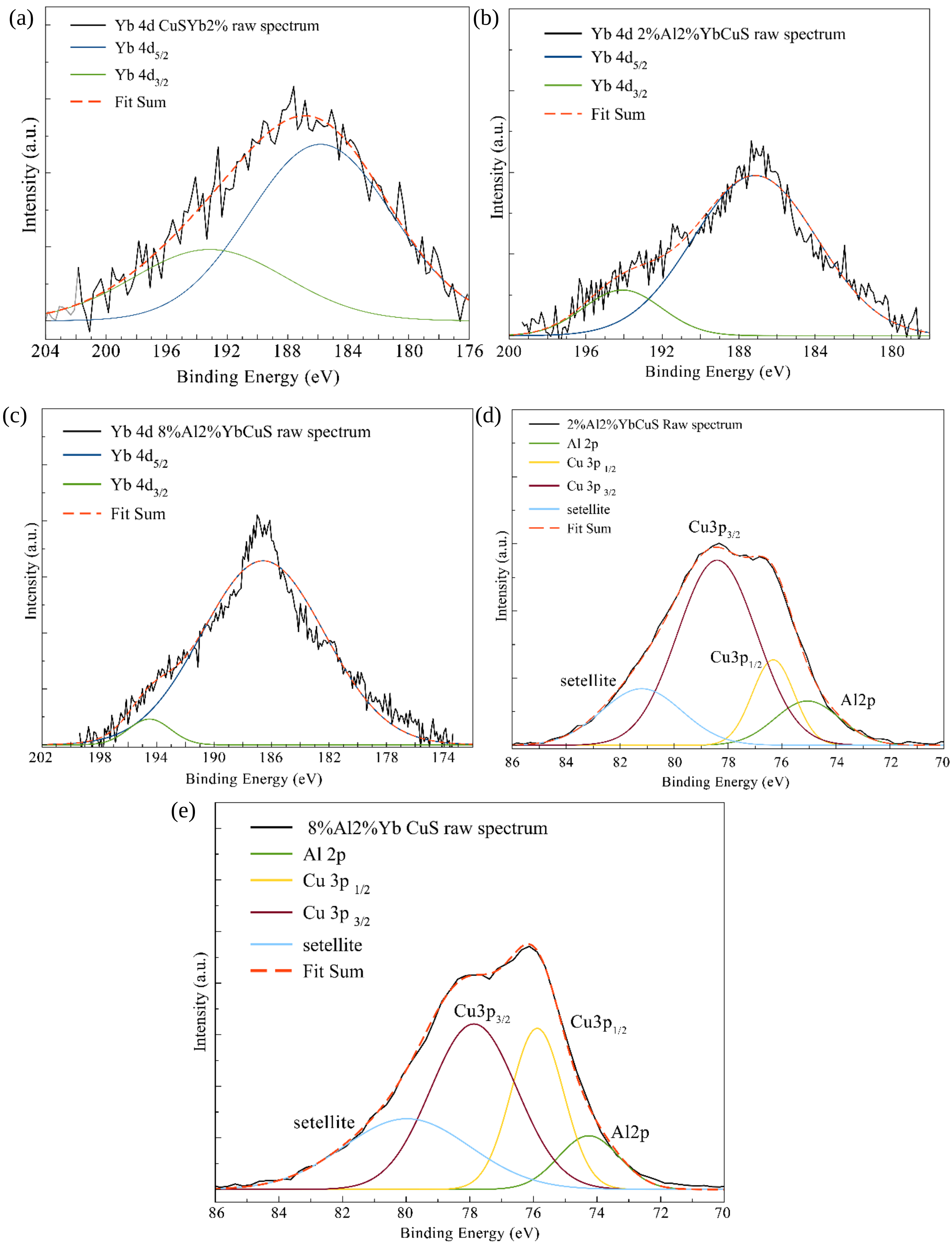

Fig. 6. Al 2p and Cu 3p core-level spectra of Yb-Al co-doped CuS nanoparticles

3.3 Chemical Analysis

X-rays photoelectron spectroscopy (XPS) was used to investigate the surface chemical composition of pristine CuS and Yb/Al co-doped CuS nanoparticle samples. The survey scan spectrum of all samples which influence of Al dopant on the changing in chemical state of CuS nanoparticles. Firstly, Figure 5 depicts the chemical composition survey scan XPS spectra of CuS and Yb/Al co-doped CuS nanoparticles. The survey scan spectra show the specific binding energy peak positions of Cu, O, C, S, Al, and Yb, indicating the existence of the primary chemical and dopant chemicals. The high-resolution narrow scan spectra of S 2p state for all samples CuS and Yb/Al co-doped CuS were illustrated in Figure 5B. The XPS spectra of S 2p located at binding energy 164.8 and 163.8 eV to confirm the S^{2-} oxidation state of covellite which correspondence with S $2p_{1/2}$ and S $2p_{3/2}$ state respectively [12]-[13]. The peak fit at binding energy 162.9 eV representing the consisting of S $2p_{3/2}$ core level for S_2^{2-} oxidation state [14]. The XPS result confirmed the oxidation state of all chemical components of pure CuS and Yb/Al co-doped CuS nanoparticles. Furthermore, Figure 5 displays the narrow scan XPS spectra of Cu 2p. The Cu 2p core-level spectra exhibit six peaks at 963.4, 955.3, 952.9, 945.3, 935.9, and 932.7 eV. The peaks at 952.9 eV and 932.7 eV were attributed to Cu^+ of Cu $2p_{1/2}$ and Cu $2p_{3/2}$, respectively, while the peaks at 955.3 eV and 935.9 eV could be assigned to Cu^{2+} of Cu $2p_{1/2}$ and Cu $2p_{3/2}$, respectively, and the peaks at 951.3 eV and 932.8 were assigned to Cu^0 of Cu $2p_{1/2}$ and Cu $2p_{3/2}$, respectively [15]. The area ratio of the Cu^+ and Cu^{2+} peaks was used to calculate the Cu^+/Cu^{2+} ratio, which is presented in table 1 shows the optical band gap of all specimens. The results demonstrated the slightly difference of optical band gap value approximately 2.28-2.30 eV. Amount of different Al loading, the Cu^+/Cu^{2+} ratio shows the decreasing with 2% Al loading. Which suggests that the Al ions replaced the Cu ions and produced holes from copper vacancies in a small and appropriate doping concentration quantity. The holes generated, increased the Cu^{2+}ions and causing the Cu^+/Cu^{2+}ratio to decrease. Meanwhile, when the amount of Al doping was too high, extra Al ions may have entered the CuS lattice's interstitial sites, producing electrons and decreasing Cu^{2+} ions, causing the Cu^+/Cu^{2+}ratio to increase.

The high-resolution spectra of Al 2p and Cu 3p orbitals were represented in Figure 6. The binding energy of Al 2p spin obit was located at 74.6 eV corelating with Al^{3+} oxidation state [16], while the strong couple peaks demonstrated at approximately binding energy 76 and 78 eV corresponding with Cu $3p_{1/2}$ and Cu $3p_{3/2}$ respectively [17]-[18]. The result demonstrated the consisting of Al dopant element on both samples of 2% and 8% Al dopant on 2%Yb doped CuS nanoparticles [19]-[21].

The small co-dopant element observation, Yb dopant element was observed by high resolution spectra as depicted in figure 6. All samples were shown a doublet spin orbit binding energy at positions 185.8 and 194.7 eV corresponding to Yb^{3+} ion with Yb $4d_{5/2}$ and Yb $4d_{3/2}$ oxidation states respectively [22]. The results suggesting that 2%Yb dopant on different loading of Al incorporated with CuS sample confirmed the Yb^{3+} ion dopant into nanoparticles [23].

Table 2. Transmission property of Al/Yb co-doped CuS particles deposited on glass substrate.

Sample	Visible transmittance (%)	NIR shielding value (%)	Spectral performance
CuS	64.3	36.5	Vis-max (64.7%)
			NIR-min (62.7%) Δ = 2.0%
CuSYbAl 2%	40.4	68.8	Vis-max (44.6%)
			NIR-min (28.9%) Δ = 15.7%
CuSYbAl 4%	70.0	37.9	Vis-max (73.2%)
			NIR-min (60.4%) Δ = 12.8%
CuSYbAl 6%	61.2	50.1	Vis-max (65.7%)
			NIR-min (47.6%) Δ = 18.0%
CuSYbAl 8%	58	53.1	Vis-max (62.5%)
			NIR-min (44.5%) Δ = 18.0%

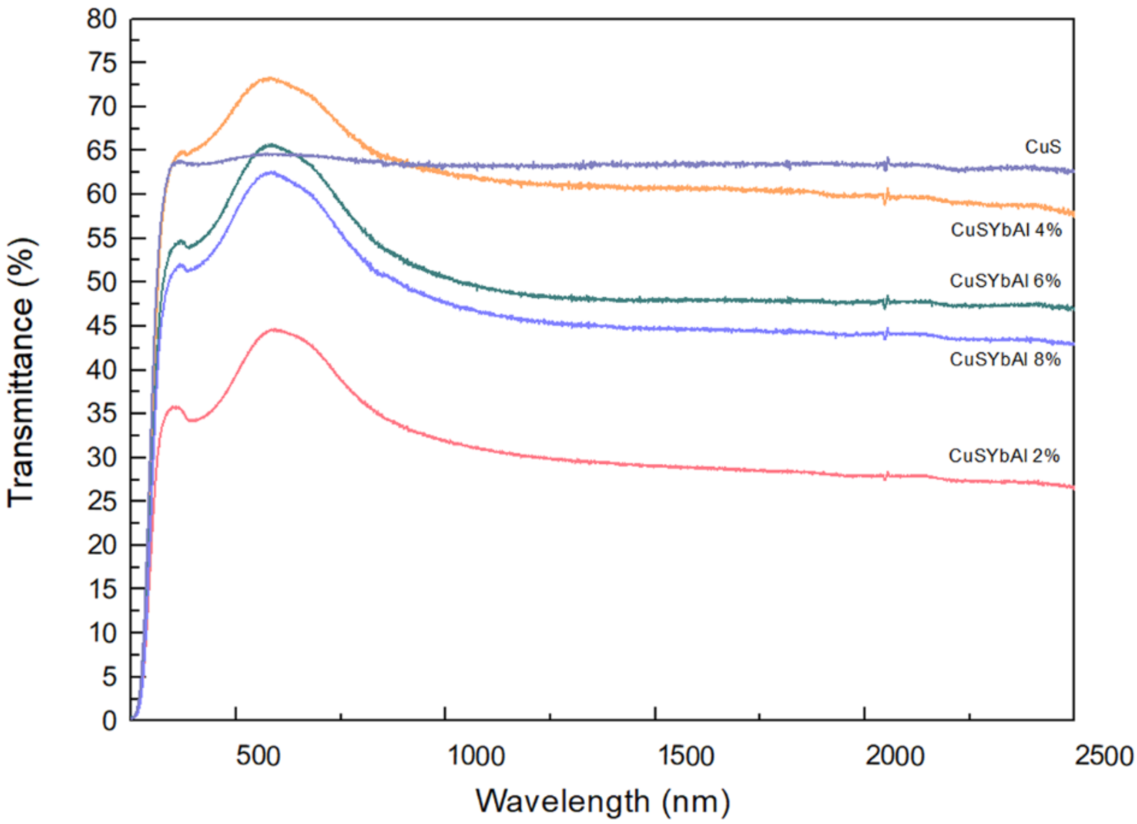

Fig. 7. UV-VIS-NIR transmittance spectra of CuS and Yb/Al co-doped CuS coated on glass substrates.

3.4 Optical properties

The UV–VIS-NIR transmission spectra of CuS and Al/Yb-doped CuS coated on glass substrate are shown in Fig. 7. The high transmittance (>50%) in visible region of 400–700 nm is observed in all samples. Moreover, there is a small noticeable absorption band covering 300-400 nm that is associated to typical interband transition of CuS. An obvious decrease in transmittance band in the region of 780–1500 nm can be obviously observed, which is attributed to optical absorption induced by localized surface plasmon resonance (LSPR). The visible light transmittance (T_{Vis}) and NIR shielding value (S_{NIR}) can be obtained by the following equations [24].

$$T_{vis} = \frac{\sum_{400}^{780} T(\lambda)}{400} \quad (1)$$

$$S_{NIR} = 1 - \frac{\sum_{780}^{1500} T(\lambda)}{400} \quad (2)$$

where T(λ) refers to the optical transmittance obtained by UV–VIS-NIR spectrometer.

In Table 2, the visible light transmittance (T_{Vis}) of undoped CuS film is found to be 64.3% while T_{Vis} of the Al/Yb co-doped CuS films is varied from 40.4% to 70.0% depending on doping contents. For S_{NIR} value, it is found that this value significantly increases when the CuS is incorporated with dopants reflecting the enhancement in infrared shielding of the sample when doped with Al and Yb. The S_{NIR} value for the doped samples varies from 36.5% to 68.8%. The optimized condition for achieving maximized spectral performance value is found in the CuSYbAl 6% providing the spectral performance value of 18.0%. The results imply that the superiority in NIR shielding ability of the Al/Yb co-doped CuS films could be related to strong photo-absorption due to LSPR phenomena that can be improved by the incorporation of Al to induced further p-type characteristic of CuS and typically strong infrared absorption feature of Yb ion [25]-[26].

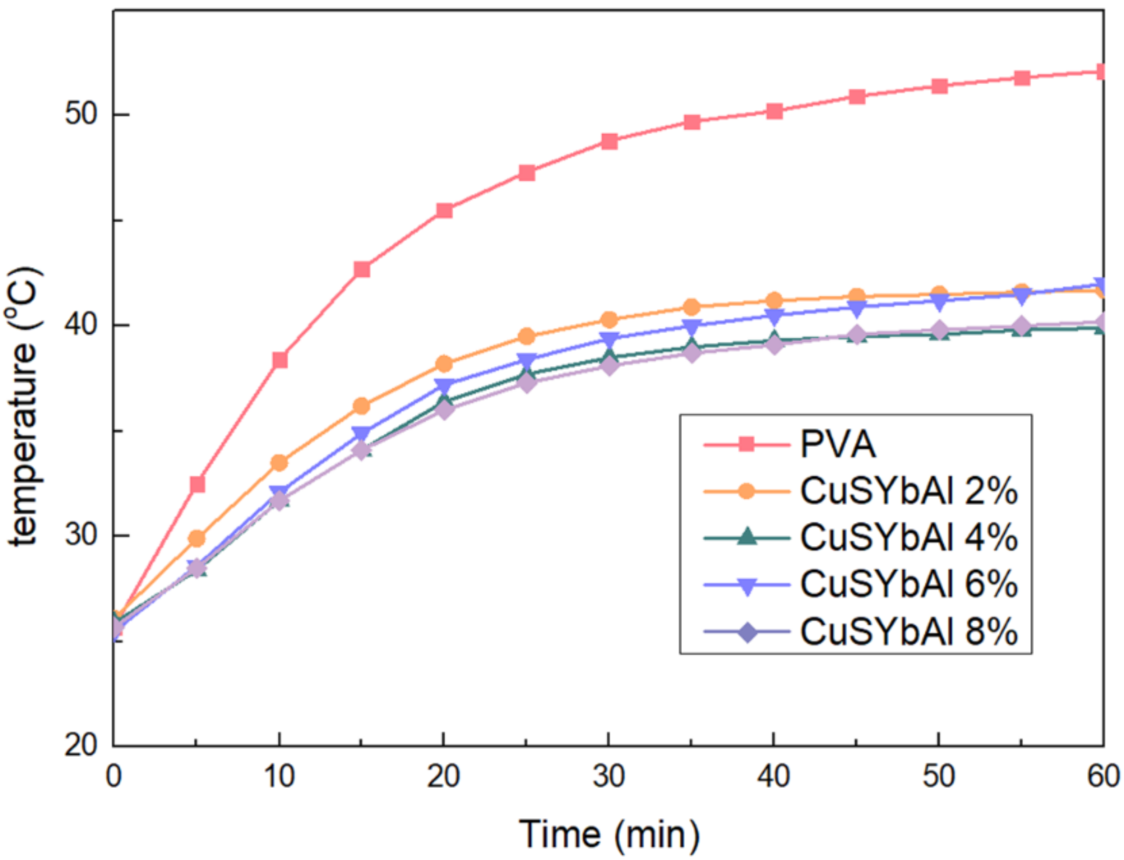

Fig. 8. The indoor temperature of the box covered with glasses coated with as-prepared Al/Yb co-doped CuS layer.

The UV–Vis–NIR spectra demonstrated enhanced absorption in the NIR region for Al/Yb dual-doped CuS compared to undoped CuS. The optimized doping composition exhibited a transmittance reduction in the NIR range, indicating superior NIR shielding performance. The observed improvements are attributed to the synergistic effects of Al and Yb doping, which modify the electronic structure and enhance light absorption.

3.5 Energy Efficiency Potential

Fig.8. shows the indoor temperature of the equipped box covered with covered by glasses coated with as-prepared Al/Yb co-doped CuS layer as a function of IR irradiation time. At first within 10 min, the indoor temperature rapidly increases from room temperature then slowly increases to reach an equilibrium temperature after irradiation for 60 min. When the PVA film glass without CuS is equipped, the indoor equilibrium temperature of the box reaches the maximum value of about 52.1°C. Meanwhile, the equilibrium temperature of in the box can be lowered to 41.7°C and 40.1°C as the box is covered by the glass coated with CuSYbAl 2% and CuSYbAl 8%, respectively. It can be deduced that the Al/Yb co-doped CuS film effectively reduces the indoor temperature of the heat box with reduction in temperature of 12°C, due to the high NIR shielding value of the Al/Yb co-doped CuS. The enhanced NIR shielding properties of Al/Yb dual-doped CuS make it a promising candidate for energy-efficient applications, particularly in smart window coatings. By reducing heat transfer through windows, these materials contribute to lower energy consumption in air-conditioned buildings.

4. Conclusion

This study successfully synthesized Al/Yb dual-doped CuS particles via a facile co-precipitation method. The dual doping approach improved the structural and optical properties of CuS, with significant enhancements in NIR shielding performance. Al dopant could enhance the LSPR-induced

NIR absorptivity of CuS while Yb dopant could further increase the NIR absorption due to characteristic transition of Yb ions. It is found that with 2% Yb doping content and 6% Al doping content results in the optimized shielding performance of CuS with spectral performance value of 18.0%. These materials have great potential for applications in energy-efficient building technologies. Future research will focus on scaling up the synthesis process and exploring the long-term stability of these materials in practical applications.

Acknowledgments

The authors acknowledge the facilities, and technical assistance from Nanotechnology and Materials Analytical Instrument Service Unit (NMIS) of College of Materials Innovation and Technology, King Mongkut Institute of Technology Ladkrabang.

References

[1] Alim, M. A., Tao, Z., Abden, M. J., Rahman, A., & Samali, B. (2020). Improving performance of solar roof tiles by incorporating phase change material. *Solar Energy, 207,* 1308-1320. DOI:10.1016/j.solener.2020.07.053.

[2] Baranowski, D., Cojocariu, I., Schio, L., Bolaños, C. G., Floreano, L., Dreiser, J., Carlotto, S., Casarin, M., Feyer, V., & Schneider, C. M. (2024). Tuning Transition Metal-Containing Molecular Magnets by On-Surface Polymerization. *Advanced Materials Interfaces, 11*(20), 2400123. DOI: 10.1002/admi.202400123.

[3] Benamra, H., Saidi, H., Attaf, A., Aida, M. S., Derbali, A., & Attaf, N. (2020). Physical properties of Al-doped ZnS thin films prepared by ultrasonic spray technique. *Surfaces and Interfaces, 21*, 100645. DOI: 10.1016/j.surfin.2020.100645.

[4] Benchouk, K., El Moctar, C., Bernede, J. C., Marsillac, S., Pouzet, J., Barreau, N., & Emziane, M. (1999). Growth and physicochemical characterization of CuAlTe2 films obtained by reaction, induced by annealing, between Cu/Al/Te/Al/Cu... Al/Cu/Al/Te layers sequentially deposited. *Journal of Materials Science, 34*(8), 1847-1853. DOI:10.1023/A:1004575612586.

[5] Cao, S., Zheng, J., Zhao, J., Yang, Z., Li, C., Guan, X., . . . Wu, T. (2017). Enhancing the Performance of Quantum Dot Light-Emitting Diodes Using Room-Temperature-Processed Ga-Doped ZnO Nanoparticles as the Electron Transport Layer. *ACS Applied Materials & Interfaces, 9*(18), 15605-15614. DOI:10.1021/acsami.7b03262.

[6] Chen, J., Xu, Z., & Chen, Y. (2020). Chapter 1 - Introduction of density functional theory. In J. Chen, Z. Xu, & Y. Chen (Eds.), *Electronic Structure and Surfaces of Sulfide Minerals* (pp. 1-12): Elsevier. DOI:10.1016/B978-0-12-817974-1.00001-6.

[7] Estrada, A. C., Silva, F. M., Soares, S. F., Coutinho, J. A. P., & Trindade, T. (2016). An ionic liquid route to prepare copper sulphide nanocrystals aiming at photocatalytic applications. *RSC Advances, 6*(41), 34521-34528. DOI:10.1039/C5RA27569E.

[8] Gao, Q., Wu, X., Fan, Y., & Meng, Q. (2018). Novel near infrared reflective pigments based on hollow glass microsphere/BiOCl1-xIx composites: Optical property and superhydrophobicity. *Solar Energy Materials and Solar Cells, 180*, 138-147. DOI:10.1016/j.solmat.2018.02.033.

[9] Ghosh, S., Saha, M., & De, S. K. (2014). Tunable surface plasmon resonance and enhanced electrical conductivity of In doped ZnO colloidal nanocrystals. *Nanoscale, 6*(12), 7039-7051. DOI:10.1039/C3NR05608B.

[10] Giribabu, K., Oh, S. Y., Suresh, R., Kumar, S. P., Manigandan, R., Munusamy, S., Gnanamoorthy, G,. Jun Y. K., Yun, S. H., & Narayanan, V. (2016). Sensing of picric acid with a glassy carbon electrode modified with CuS nanoparticles deposited on nitrogen-doped reduced graphene oxide. *Microchimica Acta, 183*(8), 2421-2430. DOI:10.1007/s00604-016-1883-7.

[11] Jiang, J., Liu, X. X., Han, J., Hu, K., & Chen, J. (2021). Self-Supported Sheets-on-Wire CuO@Ni$(OH)_2$/Zn$(OH)_2$ Nanoarrays for High-Performance Flexible Quasi-Solid-State Supercapacitor. *Processes, 9*, 680. DOI:10.3390/pr9040680.

[12] Kutwade, V. V., Gattu, K. P., Sonawane, M. E., Khan, F., Tonpe, D. A., Balal, M., Barman S. R., & Sharma, R. (2022). Growth and exploration of visible-light-driven enhanced photocatalytic

activity of Cu1–XCrxS/CdS heterojunction thin film for active dye degradation. *Applied Physics A*, *128*(7), 625. DOI:10.1007/s00339-022-05757-w.

[13] Li, X., Zhang, W., Sun, J., Liu, J., Hou, Y., Lin, L., He, K., & Yi, K. (2013). Influence of oxygen pressure and substrate temperature on the properties of aluminum fluoride thin films. *Applied Surface Science, 282*, 226-230. DOI:10.1016/j.apsusc.2013.05.108.

[14] Li, Y., Hu, J., Liu, G., Zhang, G., Zou, H., & Shi, J. (2013). Amylose-directed synthesis of CuS composite nanowires and microspheres. *Carbohydrate Polymers, 92*(1), 555-563. DOI:10.1016/j.carbpol.2012.08.102.

[15] Liu, H., Zhou, Y., Kulinich, S. A., Li, J.-J., Han, L.-L., Qiao, S.-Z., & Du, X.-W. (2013). Scalable synthesis of hollow Cu2O nanocubes with unique optical properties via a simple hydrolysis-based approach. *Journal of Materials Chemistry A, 1*(2), 302-307. DOI:10.1039/C2TA00138A.

[16] Liu, Y., Liu, M., & Swihart, M. T. (2017). Plasmonic Copper Sulfide-Based Materials: A Brief Introduction to Their Synthesis, Doping, Alloying, and Applications. *The Journal of Physical Chemistry C, 121*(25), 13435-13447. DOI:10.1021/acs.jpcc.7b00894.

[17] Mahdavi, R., & Talesh, S. S. A. (2017). Sol-gel synthesis, structural and enhanced photocatalytic performance of Al doped ZnO nanoparticles. *Advanced Powder Technology, 28*(5), 1418-1425. DOI:10.1016/j.apt.2017.03.014.

[18] Navale, S. C., Ravi, V., Mulla, I. S., Gosavi, S. W., & Kulkarni, S. K. (2007). Low temperature synthesis and NOx sensing properties of nanostructured Al-doped ZnO. *Sensors and Actuators B: Chemical, 126*(2), 382-386. DOI:10.1016/j.snb.2007.03.019.

[19] Ohno, Y. (2008). XPS studies of the intermediate valence state of Yb in (YbS)1.25CrS2. *Journal of Electron Spectroscopy and Related Phenomena, 165*(1), 1-4. DOI:10.1016/j.elspec.2008.05.009.

[20] Pacioni, N. L., Filippenko, V., Presseau, N., & Scaiano, J. C. (2013). Oxidation of copper nanoparticles in water: mechanistic insights revealed by oxygen uptake and spectroscopic methods. *Dalton Transactions, 42*(16), 5832-5838. DOI:10.1039/C3DT32836H.

[21] Ram, S., & Mondal, A. (2004). X-ray photoelectron spectroscopic studies of Al3+ stabilized t-ZrO2 of nanoparticles. *Applied Surface Science, 221*(1), 237-247. DOI:10.1016/S0169-4332(03)00883-3.

[22] Sanzaro, S., La Magna, A., Smecca, E., Mannino, G., Pellegrino, G., Fazio, E., Neri, F., & Alberti, A. (2016). Controlled Al^{3+} Incorporation in the ZnO Lattice at 188 °C by Soft Reactive Co-Sputtering for Transparent Conductive Oxides. *Energies, 9*(6). DOI:10.3390/en9060433.

[23] Singh, H., Kumar, S., Raunija, T. S. K., & Sharma, P. K. (2023). Layer hybridized exciton–plasmon resonances for enhanced dispersion modes in CuS:Al nanostructured films. *Materials Advances, 4*(20), 4877-4885. DOI:10.1039/D3MA00418J.

[24] Ubale, S. B., Kale, S. B., Mane, V. J., Bagwade, P. P., & Lokhande, C. D. (2021). SILAR synthesized nanostructured ytterbium sulfide thin film electrodes for symmetric supercapacitors. *Journal of Solid State Electrochemistry*, *25*(6), 1753-1764. DOI:10.1007/s10008-021-04941-x.

[25] Wang, J., & Shi, D. (2017). Spectral selective and photothermal nano structured thin films for energy efficient windows. *Applied Energy, 208*, 83-96. DOI:10.1016/j.apenergy.2017.10.066.

[26] Yibi, Y., Chen, J., Xue, J., Song, J., & Zeng, H. (2017). Enhancement of adjustable localized surface plasmon resonance in ZnO nanocrystals via a dual doping approach. *Science Bulletin, 62*(10), 693-699. DOI:10.1016/j.scib.2017.04.014.